DOI 10.1007/s10891-022-02462-6
Journal of Engineering Physics and Thermophysics, Vol. 95, No. 1, January, 2022

EFFECT OF OPENING PRESSURE AND AREA BLOCKAGE DUE TO OBSTACLES ON VENTED NATURAL GAS EXPLOSION

L. Pang, M. Jin, and K. Yang

UDC 532.5

The computational fluid dynamics (CFD) software FLACS is used to study the distribution of the explosion overpressure and temperature at various values of the vent opening pressure and obstacle area blockage in a typical room. The results show that obstacles cause an indoor explosion flame, severely deforming and destroying the shape of an external combustion flame. The indoor peak overpressure and peak temperature positively affect the opening pressure and obstacle area blockage. These two factors have the synergistic effect on the overpressure of the indoor gas explosion and high-temperature hazards, which exacerbates the disaster; however, in the presence of obstacles, the effect of the opening pressure on the explosion overpressure and temperature disasters is not clearly evident. Thus, indoor obstacles have a two-sided effect on the secondary external explosion and the propagation of indoor flame during a vented explosion.

Keywords: *gas explosion, vented explosion, obstacles, opening pressure.*

Introduction. Natural gas is widely used in various industrial production systems, as well as a fuel for urban residents. However, there have been frequent occurrences of accidents resulting from gas explosions owing to an inappropriate use of a natural gas or its coming in contact with a heat source or fire. Doors, windows, and light-weight walls are usually damaged in the case of a gas explosion in residential or industrial plants, thus creating vented confined explosions.

As an important characteristic parameter of a vent surface, the vent opening pressure directly affects the distribution of the indoor peak overpressure. For this reason, researchers have conducted numerous studies on the vent opening pressures [1–4]. Cao, Li, and Gao [1] found that the internal peak overpressure increases with the vent opening pressure and for higher vent opening pressures the internal pressure continues to increase within a short period of time after failure of the vent surface. McCann, Thomas, and Edwards [2] and Chow et al. [3] obtained related results. They found that an increase in the vent opening pressure leads to the peak pressure caused by gas emission that is characterized by a dominant peak. Rui et al. [4] showed that the average rate of the propagation of a flame front increases with the vent opening pressure and the overpressure curve oscillates. Most of the previous studies on the vent opening pressure have focused on small-scale experiments, so their results cannot be used to prevent or control large-scale explosions. In reality, i.e., in an actual explosion scenario, there are often many various obstacles, which significantly increases the complexity and severity of explosions. Thus it is necessary to study the effect of the vent opening pressure on explosions in the presence of such obstacles.

Obstacles are a key factor that induces turbulence in an indoor gas explosion. Numerous researchers have studied the effect of the obstacle area blockage [5, 6] on gas explosions. Oh et al. [5] pointed out that when obstacles were present, the propagation of flame fluctuated violently downstream of them. The larger was the obstacle area blockage, the higher was the increase in the speed of flame propagation. Sarli, Benedetto, and Russo [6] found that with increase in the obstacle area blockage the wall surface combustion becomes more intense and the maximum peak pressure increases. However, most of these studies were aimed at small chambers and small obstacles or sheet barriers. At the same time, studying the effect of the obstacle area blockage, the authors of a number of works often changed the obstacle volume blockage and the position of the obstacles. Thus, their studies could not comprehensively reveal the influence of the obstacle area blockage in large-scale rooms on a gas explosion.

In this study, a gas explosion in a typical large-scale room is considered as the research object, and the computational fluid dynamics (CFD) is used to study the effect of the vent opening pressure and obstacle area blockage on the explosion

School of Safety Engineering, Beijing Institute of Petrochemical Technology, 19 Qingyuan Road North, Huangcun, Daxing District, Beijing, 102617, China; email: ycyangk@bipt.edu.cn. Published in Inzhenerno-Fizicheskii Zhurnal, Vol. 95, No. 1, pp. 145–154, January–February, 2022. Original article submitted July 8, 2020.

overpressure of a vented natural gas and high-temperature disasters. The investigation and analysis, as well as the antiexplosion design, suggested in this study provide a theoretical basis for a better understanding of the phenomenon.

Numerical Model. FLACS is a three-dimensional CFD software which uses a model based on the laws of the flame development and simulates the processes of combustion and vented explosion of a combustible gas. It can describe coupled turbulence and chemical reactions and is based on the conservation equations of mass and momentum, as well as on the transport equations for enthalpy and turbulence on a three-dimensional Cartesian grid [7]. The specific representation of the governing equations is as follows:

conservation of mass

$$\frac{\partial}{\partial t}(\beta_v \rho) + \frac{\partial}{\partial x_j}(\beta_j \rho u_j) = \frac{\dot{m}}{V}; \tag{1}$$

conservation of momentum

$$\frac{\partial}{\partial t}(\beta_v \rho u_i) + \frac{\partial}{\partial x_j}(\beta_j \rho u_i u_j) = -\beta_v \frac{\partial p}{\partial x_i} + \frac{\partial}{\partial x_j}(\beta_j \rho \sigma_{ij}) + F_{oi} + F_{wi} + \beta_v(\rho - \rho_0) g_i , \tag{2}$$

where F_{oi} is the flow resistance offered by the subgrid obstructions which is given as

$$F_{oi} = -\rho \left| \frac{\partial \beta}{\partial x_i} \right| u_i |u_i| ; \tag{3}$$

transport equation for enthalpy

$$\frac{\partial}{\partial t}(\beta_v \rho h) + \frac{\partial}{\partial x_j}(\beta_j \rho u_j h) = \frac{\partial}{\partial x_j}\left(\beta_j \frac{\mu_{eff}}{\sigma_h} \frac{\partial h}{\partial x_j}\right) + \beta_v \frac{Dp}{Dt} + \frac{\dot{Q}}{V} ; \tag{4}$$

transport equation for the fuel mass fraction

$$\frac{\partial}{\partial t}(\beta_v \rho Y_{fuel}) + \frac{\partial}{\partial x_j}(\beta_j \rho u_j Y_{fuel}) = \frac{\partial}{\partial x_j}\left(\beta_j \frac{\mu_{eff}}{\sigma_{fuel}} \frac{\partial Y_{fuel}}{\partial x_j}\right) + R_{fuel} ; \tag{5}$$

transport equation for the mixture fraction

$$\frac{\partial}{\partial t}(\beta_v \rho \xi) + \frac{\partial}{\partial x_j}(\beta_j \rho u_j \xi) = \frac{\partial}{\partial x_j}\left(\beta_j \frac{\mu_{eff}}{\sigma_\xi} \frac{\partial \xi}{\partial x_j}\right). \tag{6}$$

Turbulence in an explosion of a vented gas is described by the standard k–ε turbulence model. It consists of two conservation equations for k and ε:

transport equation for the turbulent kinetic energy

$$\frac{\partial}{\partial t}(\beta_v \rho k) + \frac{\partial}{\partial x_j}(\beta_j \rho u_j k) = \frac{\partial}{\partial x_j}\left(\beta_j \frac{\mu_{eff}}{\sigma_k} \frac{\partial k}{\partial x_j}\right) + \beta_v P_k - \beta_v \rho \varepsilon ; \tag{7}$$

transport equation for the dissipation rate of this energy

$$\frac{\partial}{\partial t}(\beta_v \rho \varepsilon) + \frac{\partial}{\partial x_j}(\beta_j \rho u_j \varepsilon) = \frac{\partial}{\partial x_j}\left(\beta_j \frac{\mu_{eff}}{\sigma_\varepsilon} \frac{\partial \varepsilon}{\partial x_j}\right) + \beta_v P_\varepsilon \frac{\partial k}{\partial x_j} - C_{2\varepsilon} \beta_v \rho \frac{\varepsilon^2}{k} . \tag{8}$$

The stress tensor in the above equations is given as

$$\sigma_{ij} = \mu_{eff}\left(\frac{\partial u_i}{\partial x_j} + \frac{\partial u_j}{\partial x_i}\right) - \frac{2}{3}\delta_{ij}\left(\rho k + \mu_{eff} \frac{\partial u_k}{\partial x_k}\right), \tag{9}$$

TABLE 1. Key Parameters Used in the Numerical Simulation

Code	Physical model	Time step requirement	Boundary conditions	Initial conditions
FLACS	Navier–Stokes equations k–ε model β-flame model	CFLC[a] = 5 CFLV[b] = 0.5 NPLOT[c] = 50 DPLOT[d] = 0.025	Euler	Velocity fluctuation of 0 m/s Initial turbulence length scale of 0 m $T = 20^{o}$C

[a]Courant–Friedrichs–Levy (CFL) number based on the sound speed.

[b]CFL number based on the flow velocity.

[c]Parameter that may be used to determine how often the data for the field plots are written to a file during simulation.

[d]Time interval for the field output (in s).

TABLE 2. Simulation Results for the Maximum Peak Pressure under Different Boundary Conditions

Computational domain, m^3	Euler conditions, kPa	Plane wave conditions, kPa	Absolute discrepancy	Relative discrepancy, %
10 × 15.5 × 15.5	188.00	189.60	1.6	0.84
15 × 15.5 × 15.5	188.24	189.59	1.35	0.71
20 × 15.5 × 15.5	188.56	188.66	0.1	0.05
25 × 15.5 × 15.5	188.63	188.49	0.14	0.07
30 × 15.5 × 15.5	188.64	188.59	0.05	0.03
Max absolute discrepancy	0.64	1.11	–	–
Max relative discrepancy, %	0.34	0.59	–	–

where

$$\mu_{\text{eff}} = \mu + \rho C_{\mu} \frac{k^2}{\varepsilon} . \tag{10}$$

Here the second term is known as the turbulent (or eddy) viscosity.

Model Validation. Tomlin et al. [8] conducted a large-scale vented natural gas/air explosion experiment, using an experimental device with the dimensions 9.0 m × 4.5 m × 4.5 m. The results obtained with the numerical model were compared with the data of this experiment for verification of the model. The values of the key parameters used in the simulation are summarized in Table 1. The explosion venting area was 5.06 m^2, the methane concentration was stoichiometric, and the ignition point was located at 0.25 m from the geometric center of the rear wall.

To study the influence of boundary conditions and computational domain on the simulation results [9], two types of boundary conditions, namely, the Euler and plane wave ones, were selected. The length in the x direction was set as 10, 15, 20, 25, and 30 m to validate the computational domain size. The experimental data were taken from the same indoor measurement point (0.4 m away from the rear wall). The indoor maximum peak overpressures are presented in Table 2. The results indicate that both types of boundary conditions and five computational domains are suitable to this study. Therefore, henceforward in this study only the Euler boundary conditions are used. In addition, to completely cover the outdoor explosion, the computational domain size was set as 30 m × 15.5 m × 15.5 m.

Next the grid sensitivity in simulating the explosion was analyzed. From the recommendation of [7] regarding the grid size which should be at least 0.2 m during the gas explosion simulations, five different grid sizes were selected.

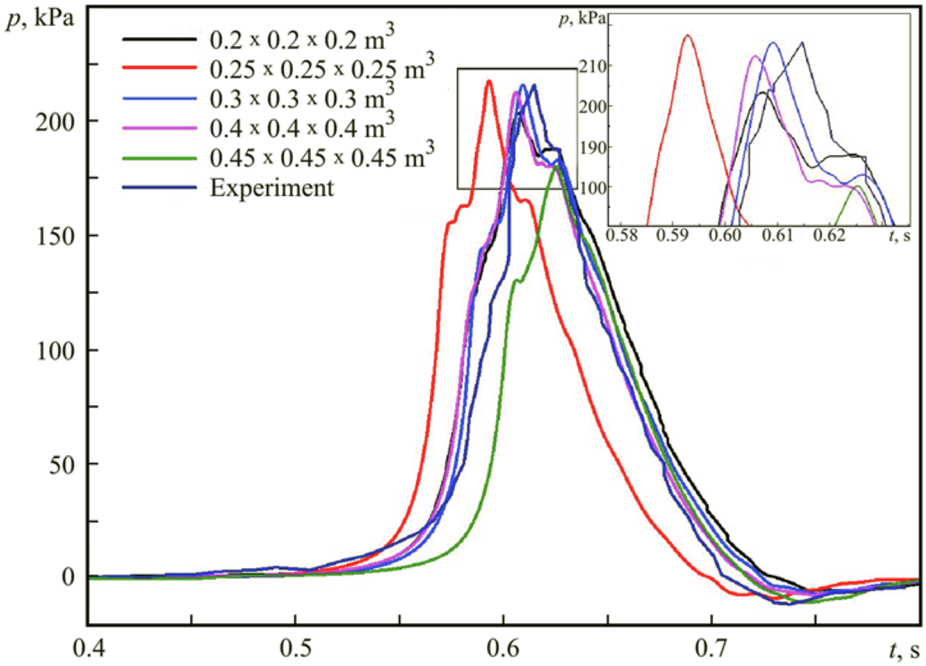

Fig. 1. Overpressure obtained from the numerical simulation with various grid sizes and from the experiments.

TABLE 3. Numerical and Experimental Overpressures

Grid size, m	Overpressure, kPa	Absolute discrepancy	Relative discrepancy, %	Peak overpressure arrival time, s	Absolute discrepancy	Relative discrepancy, %
Experiment	206.29	–	–	0.6133	–	–
0.2	203.29	3.00	1.45	0.6070	0.0063	1.02
0.25	217.49	11.20	5.15	0.5927	0.0206	3.36
0.3	215.66	9.37	4.34	0.6091	0.0114	1.86
0.4	212.35	6.06	2.85	0.6057	0.0076	1.24
0.45	180.20	26.09	12.65	0.6252	0.0119	1.90

The simulation conditions are same as those used in the experiment of Tomlin et al. [8]. Figure 1 enables one to compare the overpressure curves obtained from the numerical calculation with the experimental results for different grid sizes, and Table 3 summarizes the corresponding discrepancy data. It can be seen that for different grid sizes the trends of the overpressure curves obtained from the numerical simulations and from the experiments are fundamentally the same. The comparative discrepancy analysis shows that at the grid size 0.2 m the indoor maximum peak overpressure and its arrival time are characterized by the smallest deviation from the corresponding experimental results. Therefore, a comparison between the results of the experiments and numerical simulations and the verification of the results suggest that the aforementioned numerical method offers a feasible solution of the transient problem for a vented explosion flow field in a large-scale room with obstacle blockages. Based on this analysis, the grid size 0.2 m was employed for all subsequent simulations.

Research Plan. The size of the room model selected in this study was 9 m × 4.5 m × 4.5 m. It was equipped with a vent of a square cross section with a venting area of 5.06 m^2. The ignition point was located on the geometric centerline and 0.25 m away from the rear wall of the room. The computational domain was extended outward beyond the vent by

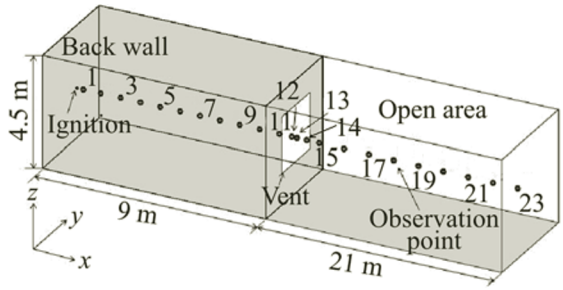

Fig. 2. Schematic diagram for the numerical simulation.

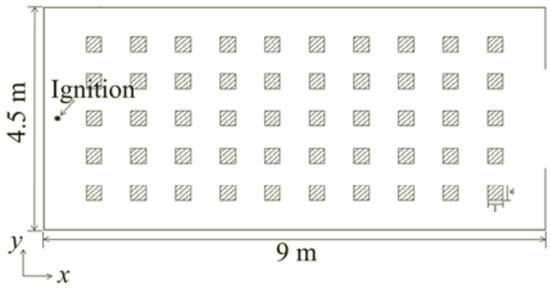

Fig. 3. Schematic diagram of the layout of the obstructions.

TABLE 4. Specific Simulation Conditions at the Volume Blockage 5%

Test No.	Sectional area of each obstacle, m^2	Area blockage, %	Vent opening pressure, kPa
1	0.2025 × 0.2	22	10
2	0.2025 × 0.2	22	20
3	0.2025 × 0.2	22	30
4	0.2025 × 0.2	22	40
5	0.2025 × 0.2	22	50
6	0.135 × 0.3	33	10
7	0.10125 × 0.4	44	10

a distance of 2.3 times greater than the room length to capture the effects of external explosions. The room was filled with a methane–air mixture of stoichiometric concentration. All the measurement points were located on the geometric centerline of the model, as shown in Fig. 2. The opening pressure of the explosion-venting surface varied in the range 10–50 kPa. The number of indoor obstacles and their arrangement remained unchanged throughout the simulations. The specific arrangement is shown in Fig. 3. The height of the obstacles was 4.5 m and different obstacle area blockages could be set by changing the length l and the width w of the obstacles. The specific simulation conditions, i.e., the values of $l \times w$, are summarized in Table 4.

Typical Process of Vented Gas Explosion in the Room under the Influence of Obstacles. Figure 4 shows the overpressure–time curves at each measurement point in the room and at the points close to the vent outside the room at the opening pressure 30 kPa. It can be seen from Fig. 4a that three types of the overpressure peaks are observed in the overpressure–time curves. The first overpressure peak p_1 appeared 0.67–0.68 s after the explosion occurrence, which corresponded to the vent opening. At this time, the difference between the pressures inside and outside the room was small; the rate of outward diffusion of an unburnt gas was low and the resulting pressure peak value was not significant. The second overpressure peak p_2 appeared immediately after p_1. This was a group of the Helmholtz oscillation peaks whose formation could be explained as follows. Firstly, the combustion gas reached the plane where the vent was located and began to exhaust outwards. The volume flow rate is inversely proportional to the square root of the exhaust gas density; therefore, when the density of the combustion gas discharged from the vent was reduced, the volume flow rate increased sharply. Meanwhile, the amount of a gas discharged in a short time would far exceed the amount of a gas generated by combustion, resulting in the decrease in the pressure inside the room. Consequently, the original differential pressure in the room is reduced, which in turn decreases the outward flow rate of the gas and causes the pressure in the room to increase, thus creating a cycle of the pressure fluctuations. The third overpressure peak p_3 appeared after 0.75–0.8 s. It may be caused by an external explosion, the Helmholtz effect, and the Taylor instability. Owing to the rear wall ignition, a large amount of the unburnt gas was discharged through the vent and accumulated outside it. Turbulence generated by the obstacles caused

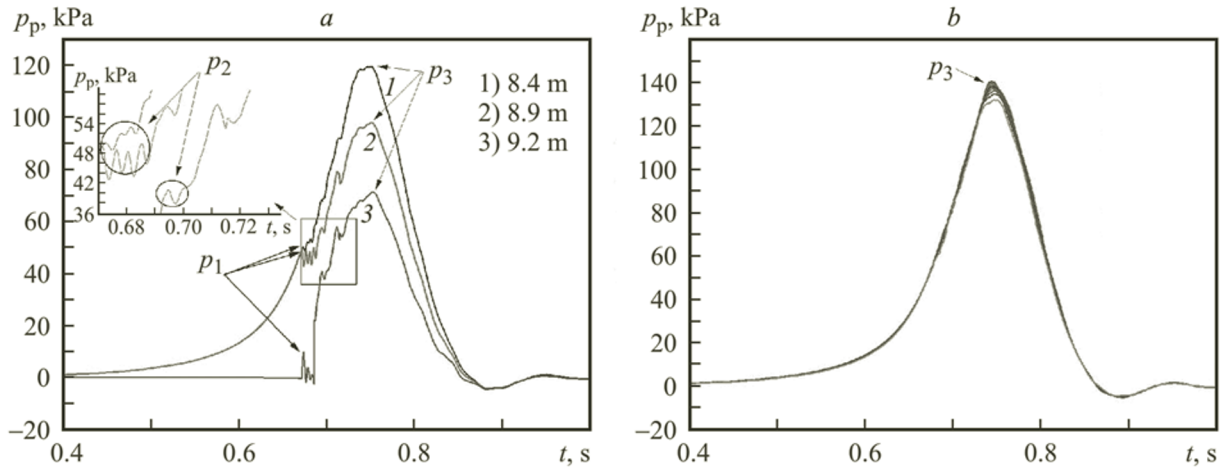

Fig. 4. Time dependences of the explosion overpressure under an opening pressure of 30 kPa in the ranges 8.4–9.2 m (a) and 0.4–7.6 m (b).

a strong external explosion. At the same time, owing to the low combustion gas density, when the high-velocity combustion gas entered a relatively dense low-velocity mixture of the unburnt gas and air, the boundary layer would produce the Taylor instability, leading to the large increase in the flame surface area. This would result in a larger overpressure peak, when the flame propagated to the surrounding wall. Bauwens et al. [10, 11] concluded that obstacles had a greater impact on the peaks caused both by external explosions and by an increased flame surface area.

As shown in Fig. 4b, the overpressure–time curves of the indoor measuring points sufficiently far away from the vent have only one peak. This is because turbulence caused by the obstacles results in the increase in the flame area of the indoor gas combustion and thus to the increase in the combustion rate. The reduction of the amount of gas caused by the explosion does not significantly affect the indoor pressure, i.e., the gas release rate is much less than the generation rate. In a short period of time, the amount of an internal generated gas is greater than that of a discharged one. This phenomenon was also found experimentally by Chen et al. [12].

Figure 5 shows the contour map distributions of the combustion products under an opening pressure of 30 kPa at different times selected to capture the characteristics of the flame propagation of a typical process for the vented confined explosion. In Fig. 5a and b, the flame front had not reached the first row of obstacles, and the flame structure was similar to a hemisphere. Then, as seen from Fig. 5c and d, the flame continued to propagate forward and passed through the obstacles. Owing to obstruction and turbulence induced by the obstacles, the arc-shaped flame front was folded and deformed; it became sagged, and the flame propagation speed increased gradually. Fig. 5e corresponds to 0.68 s, at this instant the indoor overpressure reached the opening pressure. The opening of the vent surface caused the indoor gas to be discharged through the vent, generating the first peak value p_1. Under the influence of the obstacles in the middle of the room, concave deformation of the flame front became more obvious. Figure 5g and h shows that the flame violently burnt outdoors, forming a secondary explosion. The outdoor flame front was deformed under the action of the air resistance, and the front end was deflected by the flame, turning outwards on both sides. The air entrained in the flame diluted the fuel and formed a continuous vortex, manifesting the Helmholtz effect. The corresponding time in Fig. 5i was 0.78 s. At this time, the indoor flame area continued to increase, extending to the wall where the vent surface was located. The flame area reached its maximum value, forming the overpressure peak p_3. Finally, the external combustion gas was diluted, thus effectively reducing the risk of an external secondary explosion. Therefore, further research is needed on using different types of obstacles to prevent the formation of an external combustible gas.

In Fig. 6, the flame speed is presented. It can be seen that the larger the number of obstacles passed, the more obvious the increase in the flame speed. It is basically consistent with the phenomenon described by the contour maps of the combustion products.

Figure 7a shows the change in the peak overpressure versus x under different vent opening pressures at the obstacle area blockage (AB) indoors 22% and the obstacle volume blockage (VB) 5%. The peak overpressure reaches a maximum value indoors and decreases with the distance. As the opening pressure increases from 10 to 50 kPa, the maximum peak

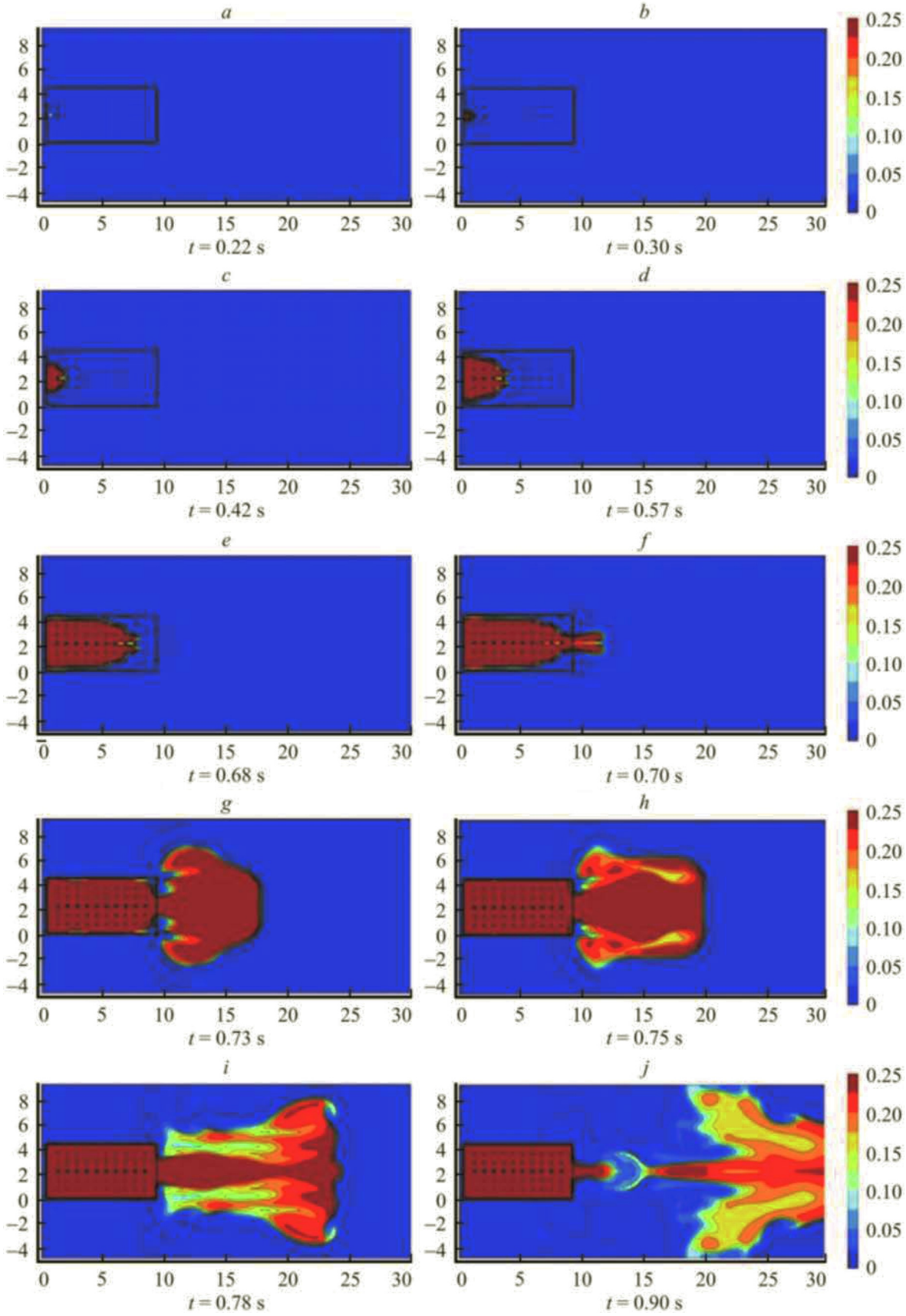

Fig. 5. Nephograms of explosion combustion product at different times.

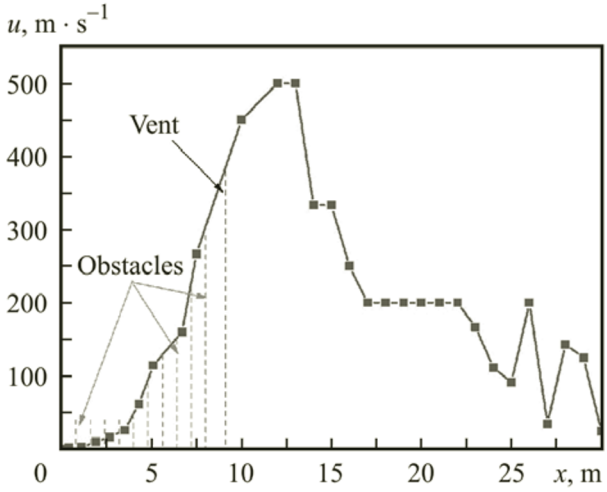

Fig. 6. Explosion flame speed at an opening pressure of 30 kPa.

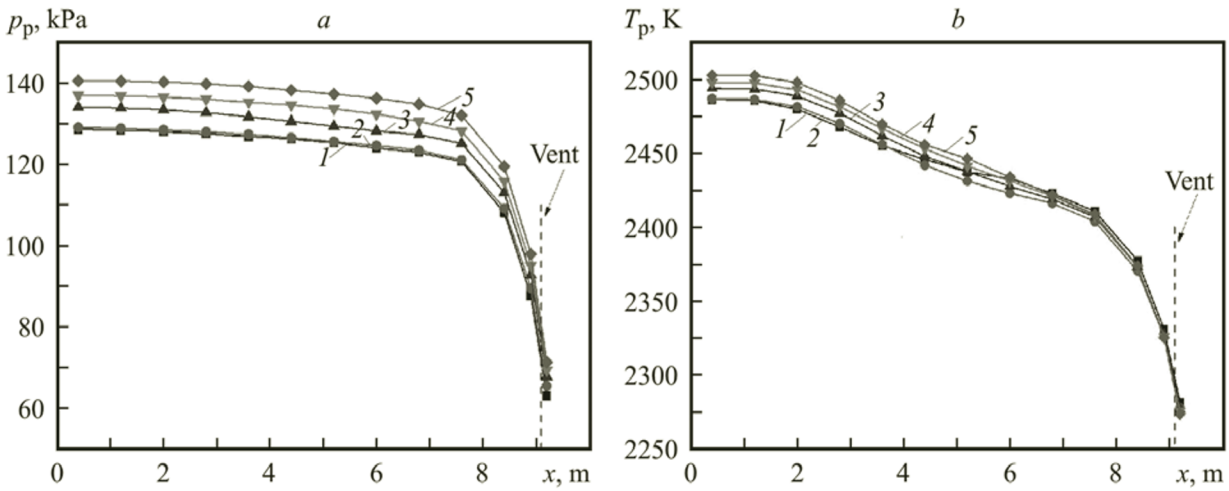

Fig. 7. Explosion peak overpressure (a) and temperature (b) vs. x at AB = 22%, VB = 5%, and various opening pressures: 10 (1), 20 (2), 30 (3), 40 (4), and 50 kPa (5).

overpressure increases from 128.57 to 140.57 kPa, i.e., the growth is 9.33%. This is because the larger the opening pressure, the greater the pressure difference between the inside and outside the room at the moment when the explosion surface is opened and the greater the turbulence intensity caused by the indoor gas discharge; therefore, the combustion rate of the indoor gas increases, resulting in a greater peak overpressure [13].

Indoor Hazards of Vented Gas Explosion. Figure 7b shows the change in the peak temperature with x under different vent opening pressures at the obstacle AB 22% and the obstacle VB 5% indoor. The maximum indoor peak temperature was obtained near the rear wall. This is because as the vent opening pressure increases, the combustible gases produce more chemical reactions in the room, which promotes the increase in the indoor peak temperature.

Figure 8a gives the peak overpressure with x at different distances for different obstacle AB values at the obstacle VB maintained equal to 5%. The maximum peak overpressure reaches a maximum value indoors and then increases with the obstacle AB. As the obstacle AB increases from 22 to 44%, the maximum peak overpressure increases from 128.57 to 328.27 kPa, i.e., the increase is equal to 155.32%. On the one hand, as the obstacle AB increases, the horizontal distance between any two obstacles decreases; the greater the squeezing effect on the flame propagation in the direction of the vent, the higher the flame deformation, which significantly increases the flame surface area, resulting in the increase in the combustion rate of the combustible gas. On the other hand, when the flame reaches this turbulent area, the heat and mass

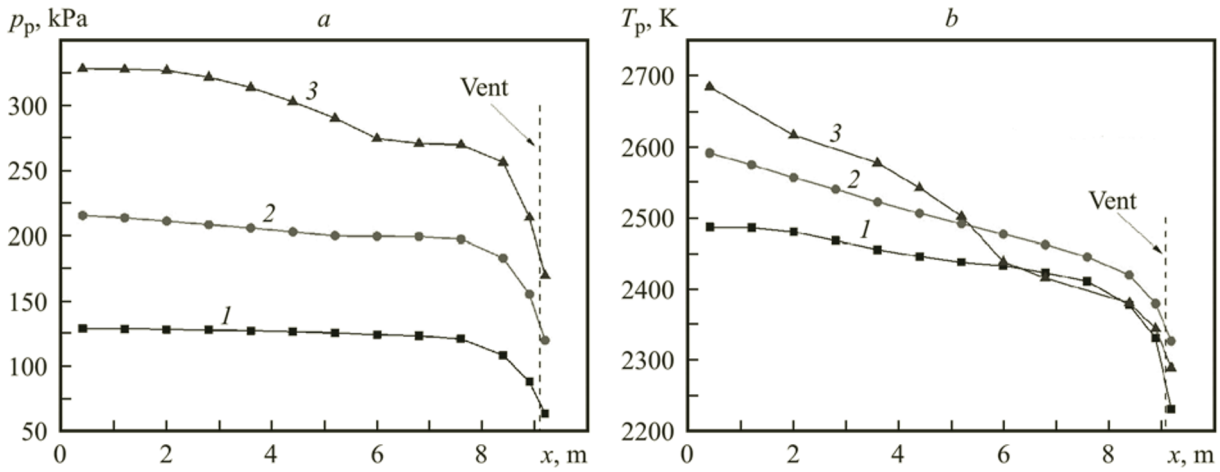

Fig. 8. Explosion peak overpressure (a) and temperature (b) vs. x at VB = 5% and various obstacle AB values: 22 (1), 33 (2), and 44% (3).

transfer rate in the reaction zone increases, which causes a rapid increase in the combustion speed and eventually leads to an increase in the overpressure [14].

Figure 8b gives the peak temperature along the x axis at different values of the obstacle AB at the obstacle VB equal to 5%. The maximum peak temperature is obtained near the back wall, and it increases with the obstacle AB. The trend of the peak temperature change is slightly different from that obtained with an obstacle AB of 44%. This may be due to the influence of the obstacles on the flame in the process of propelling the gas in the room forward. As a result, a higher pressure gradient is formed on the obstacle surface [15]. This reduces the flame propagation speed and obstructs the explosion development.

Conclusions. Obstacles can effectively promote gas combustion, increase the speed of the flame propagation, and make the flame front folded and deformed. Further researches are needed on the formation of outdoor flammable gas clouds to prevent external explosions due to the destruction of the flames and flammable gas clouds by the obstacles.

Compared with turbulence induced by the vent opening, turbulence induced by obstacles plays a dominant role. The overpressure in an explosion of a vented natural gas and high-temperature disasters have a strong positive correlation with the obstacle AB. However, when the obstacle AB increases beyond a particular value, the obstacles may block the flame propagation. Therefore, the mechanism of the influence of obstacles in typical building structures on vented gas explosion invites further study.

The obstacles and the vent opening pressure have a synergistic effect on a confined explosion of a vented natural gas and at the same time promote an increase in the explosion overpressure and temperature; however, the presence of obstacles will weaken the impact of the vent opening pressure on the indoor explosion overpressure and high-temperature disasters. In the investigation of gas explosion accidents and disaster prevention, it is necessary to investigate the relationship between the obstacles and vent surface.

Acknowledgments. The authors appreciate the financial support received from the Beijing Natural Science Foundation–Municipal Education Committee Joint Funding Project (No. KZ201910017020); the Training Funded Project of the Beijing Youth Top-Notch Talents of China (No. 2016000026833ZK05); Science and Technology Plan Project of Beijing Education Commission (No. KM202010017008), and the Training Funded Project of the Beijing Young Backbone Talents of China (No. 2018000020124G087).

NOTATION

C_μ, model constant; F_{wi}, flow resistance offered by the walls; F_{oi}, flow resistance offered by the subgrid obstructions; g, gravitational acceleration; h, specific enthalpy; k, turbulent kinetic energy; $\dot{m}$, mass rate; p, static pressure; P, gauge pressure; $\dot{Q}$, heat flow rate; R_{fuel}, fuel reaction rate; t, time; u, velocity; V, volume; x, space coordinate; Y_{fuel}, fuel mass fraction; β, area porosity; β_v, volume porosity; ε, dissipation rate; μ_{eff}, effective viscosity; ξ, mixture fraction; ρ, density;

σ_{ij}, stress tensor components; σ_ε and $C_{2\varepsilon}$, adjustable constants. Indices: *i* and *j*, associated coordinates; o, obstruction; w, wall.

REFERENCES

1. Y. Cao, B. Li, and K. H. Gao, Pressure characteristics during vented explosion of ethylene–air mixtures in a square vessel, *Energy*, **151**, 26–32 (2018).
2. D. P. J. McCann, G. O. Thomas, and D. H Edwards, Gas dynamics of vented explosions. Part I. Experimental studies, *Combust. Flame*, **59**, 233–250 (1985).
3. S. K. Chow, R. P. Cleaver, M. Fairweather, and D. G. Walker, An experimental study of vented explosions in a 3:1 aspect ratio cylindrical vessel, *Process Saf. Environ. Prot.*, **78**, 425–433 (2000).
4. S. C. Rui, J. Guo, G. Li, and C. J. Wang, The effect of vent burst pressure on a vented hydrogen–air deflagration in a 1 m^3 vessel, *Int. J. Hydrog. Energy*, **43**, 21169–21176 (2018).
5. K. H. Oh, H. Kim, J. B. Kim, and S. E. Lee, A study on the obstacle-induced variation of the gas explosion characteristics, *J. Loss Prev. Proc. Ind.*, **14**, 597–602 (2001).
6. V. D. Sarli, A. D. Benedetto, and G. Russo, Using large eddy simulation for understanding vented gas explosions in the presence of obstacles, *J. Hazard. Mater.*, **169**, 435–442 (2009).
7. *GexCon AS. FLACS Version 10.7 User's Manual*, GEXCON AS, Bergen (2017), pp. 389–390.
8. G. Tomlin, D. M. Johnson, P. Cronin, H. N. Phylaktou, and G. E. Andrews, The effect of vent size and congestion in large-scale vented natural gas/air explosions, *J. Loss Prev. Proc. Ind.*, **35**, 169–181 (2015).
9. K. Yang, P. F. Lv, J. C. Gao, and L. Pang, Influence of the region outside a vent on the explosion of an indoor gas, *J. Eng. Phys. Thermophys.*, **93**, 466–473 (2020).
10. C. R. Bauwens, J. Chao, and S. B. Dorofeev, Effect of hydrogen concentration on vented explosion overpressures from lean hydrogen–air deflagrations, *Int. J. Hydrog. Energy*, **37**, 17599–17605 (2012).
11. C. R. Bauwens, J. Chaffee, and S. Dorofeev, Effect of ignition location, vent size, and obstacles on vented explosion overpressures in propane–air mixtures, *Combust. Sci. Technol.*, **182**, 1915–1932 (2010).
12. Y. Chen, Z. T. Li, C. Ji, and X. Y. Liu, Effects of hydrogen concentration, nonhomogeneous mixtures and obstacles on vented deflagrations of hydrogen–air mixtures in a 27 m^3 chamber, *Int. J. Hydrog. Energy*, **45**, 7199–7209 (2020).
13. Y. Cao, B. Li, and K. Gao, Pressure characteristics during vented explosion of ethylene–air mixtures in a square vessel, *Energy*, **151**, 26–32 (2018).
14. D. Y. Chen, L. J. Zhang, G. Tao, and F. Yang, Study of obstacles to flame propagation in process of the combustible gas explosion, *Ind. Saf. Environ. Prot.*, **38**, 35–37 (2012).
15. Y. H. Liu and Y. B. Ding, Effects of different blocking ratios of three-dimensional structural obstacles on flame propagation, *Hunan Nonferrous Met.*, **1**, 1–4 (2008).